Supplementary Information (SI) for Journal of Materials Chemistry A.

Supporting Information

Harnessing Self-powered and Photoresponsive Biomechanical Activity Sensors by Exploring Piezo-phototronic Effect in Lead-free Layered Halide Perovskite/PVDF Composites

Prabhat Kumar[1], Tufan Paul[1], Aditi Sahoo[1], Manoj Singh[1], Arupjyoti Pathak[2], Ranjit Thapa[2,3], and Rupak Banerjee[1,4*]

[1] *Department of Physics, Indian Institute of Technology Gandhinagar, Palaj 382355, Gujarat, India.*

[2] *Department of Physics, SRM University AP, Amaravati 522240, Andhra Pradesh, India*

[3] *Centre for Computational and Integrative Sciences, SRM University -AP, Amaravati 522240, Andhra Pradesh, India*

[4] *K C Patel Centre for Sustainable Development, Indian Institute of Technology Gandhinagar, Palaj 382355, Gujarat, India*

*Corresponding author E-mail: rupakb@iitgn.ac.in

Synthesis of $Cs_3Sb_2I_9$ perovskite:

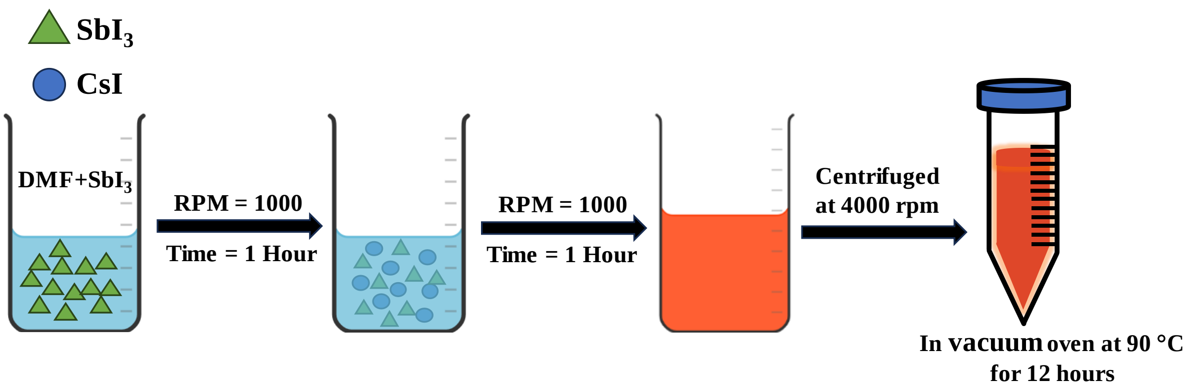

Figure S1: *Synthesis of $Cs_3Sb_2I_9$*

Preparation of the composite:

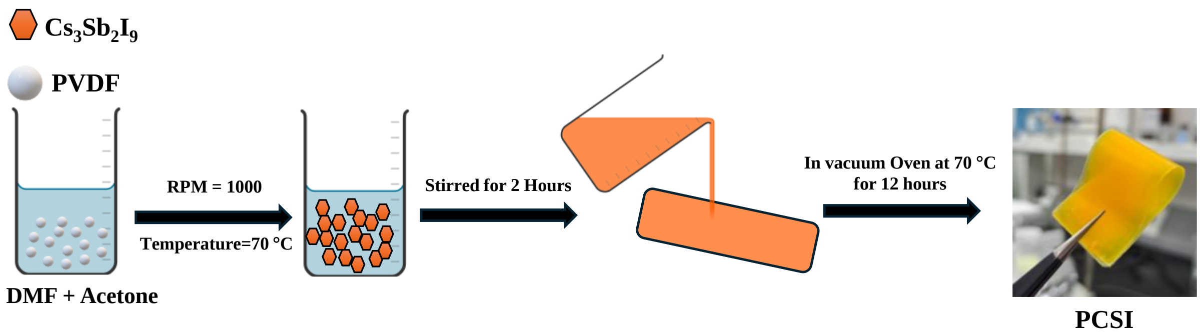

Figure S2: *Schematic for the synthesis of the composite of* $Cs_3Sb_2I_9$ *and PVDF (PCSI).*

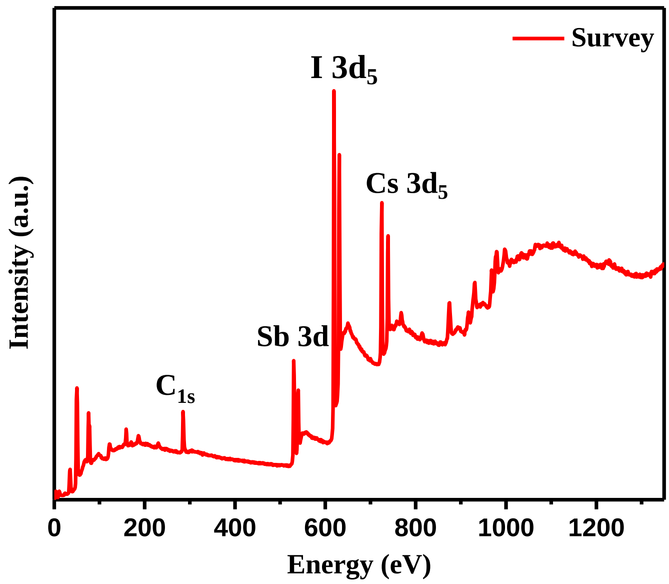

Figure S3: *XPS survey scan of* $Cs_3Sb_2I_9$

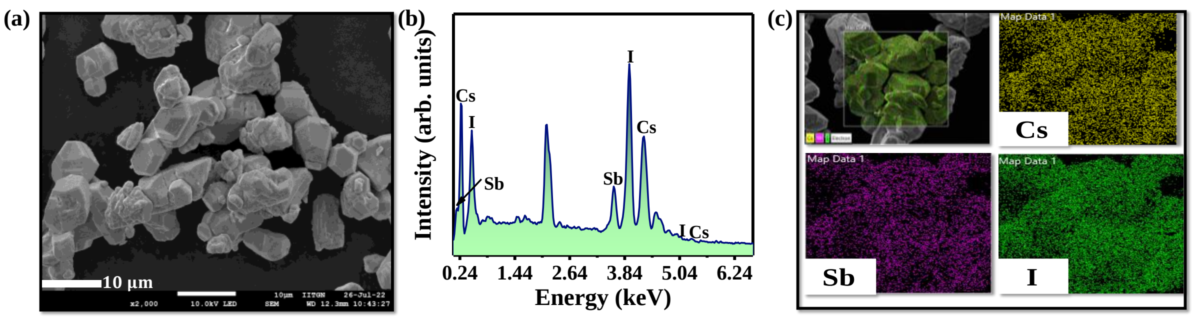

Figure S4: *(a) The FESEM image (b) The EDX spectra (c) EDX elemental distribution*

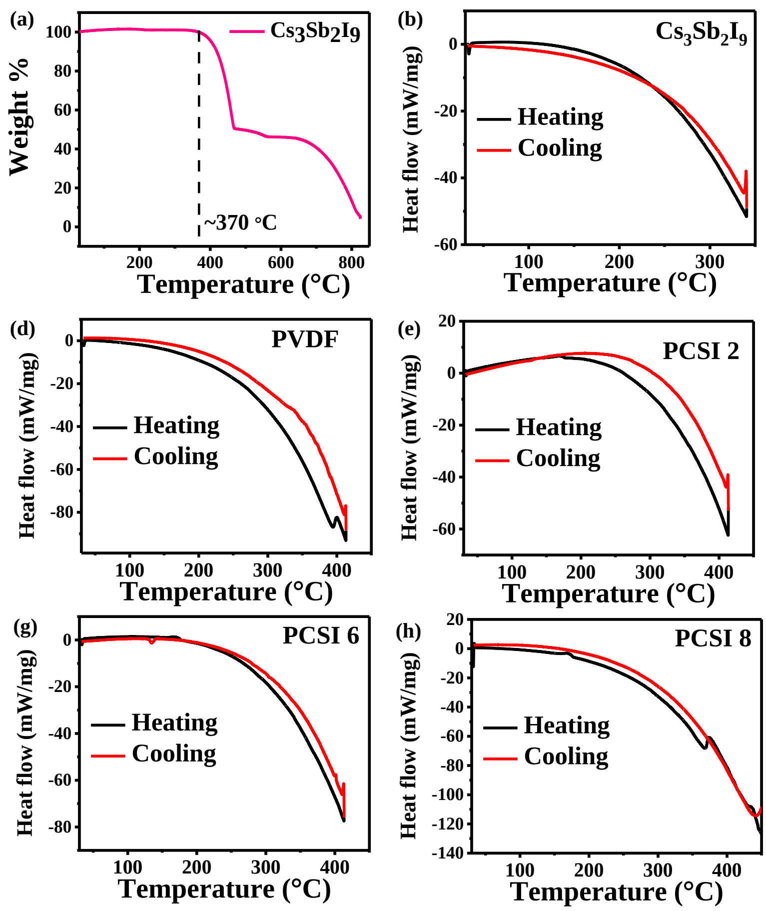

Figure S5: *(a) TGA and (b) DSC of $Cs_3Sb_2I_9$, (c) TGA of PVDF and composites, DSC curve of (d) PVDF, (e) PCSI 2, (f) PCSI 4, (g) PCSI 6, (h) PCSI 8, and (i) PCSI 10.*

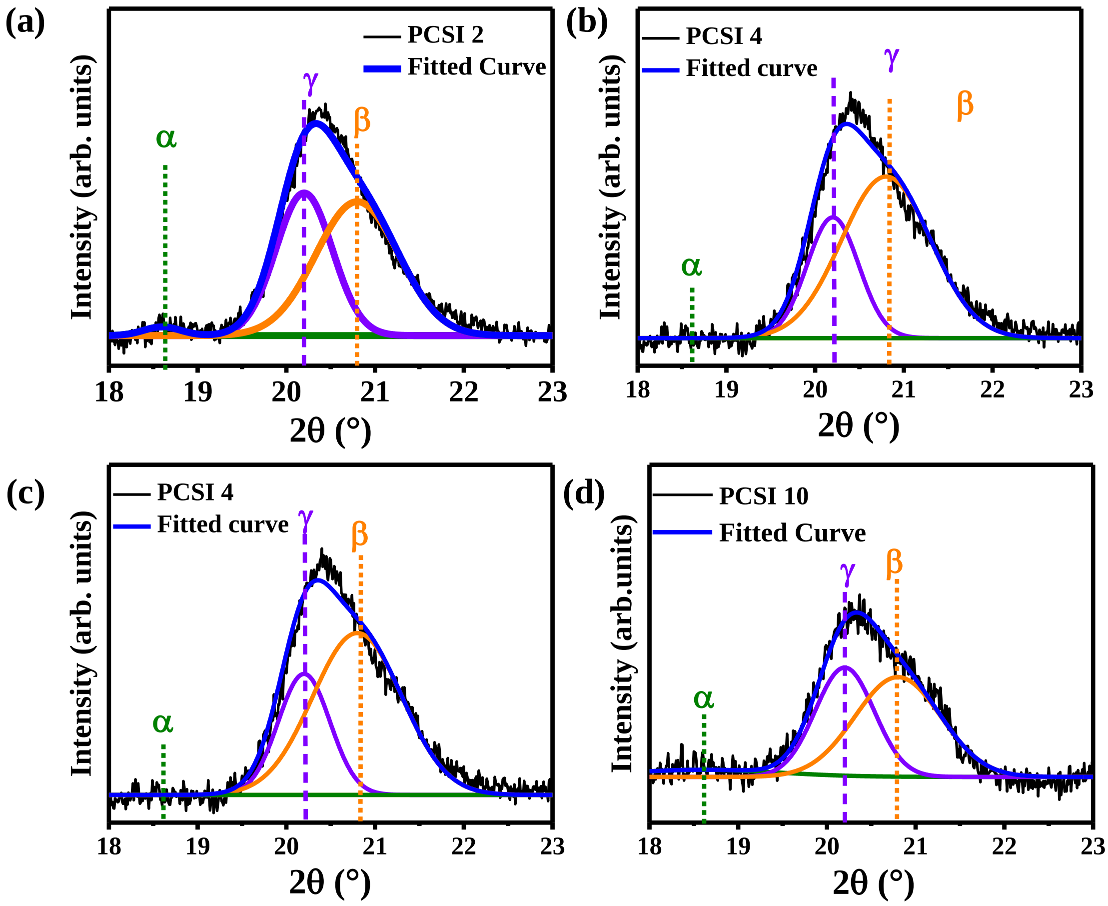

Figure S6: *The deconvoluted XRD profiles showing α, β, and γ-phases of (a) PCSI2, (b) PCSI4, (c) PCSI6, and (d) PCSI10*

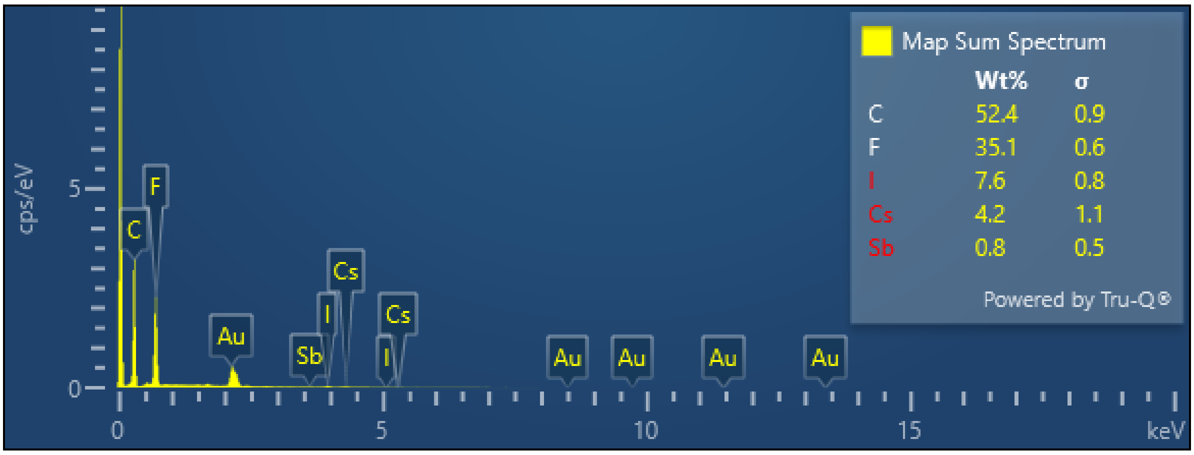

Figure S7: *EDX Spectra of PCSI8*

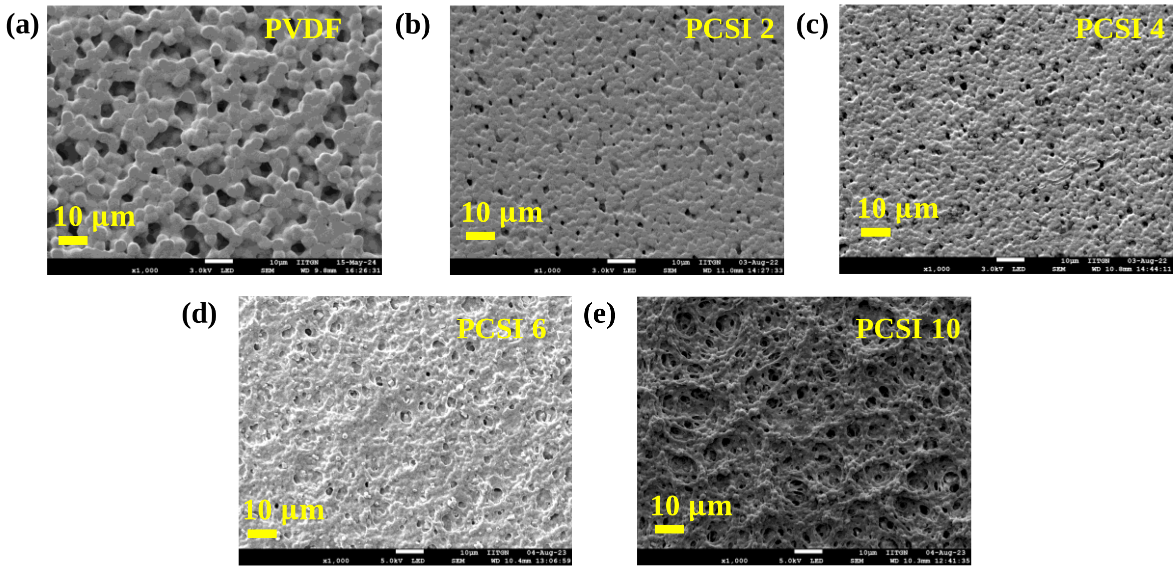

Figure S8: *FESEM images of (a) PVDF, (b) PCSI2, (c) PCSI4, (d) PCSI6, and (e) PCSI10*

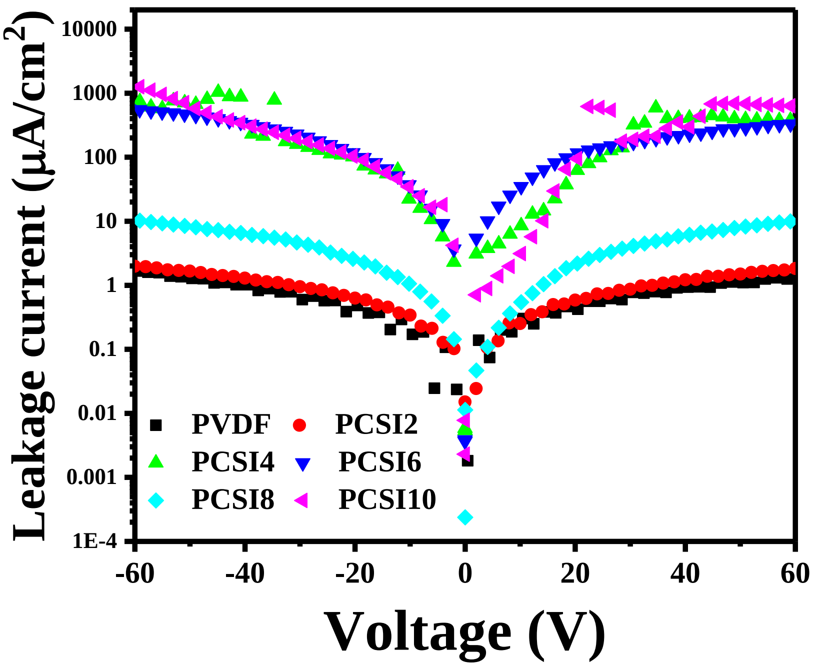

Figure S9: *Leakage current density of PVDF and all the composites.*

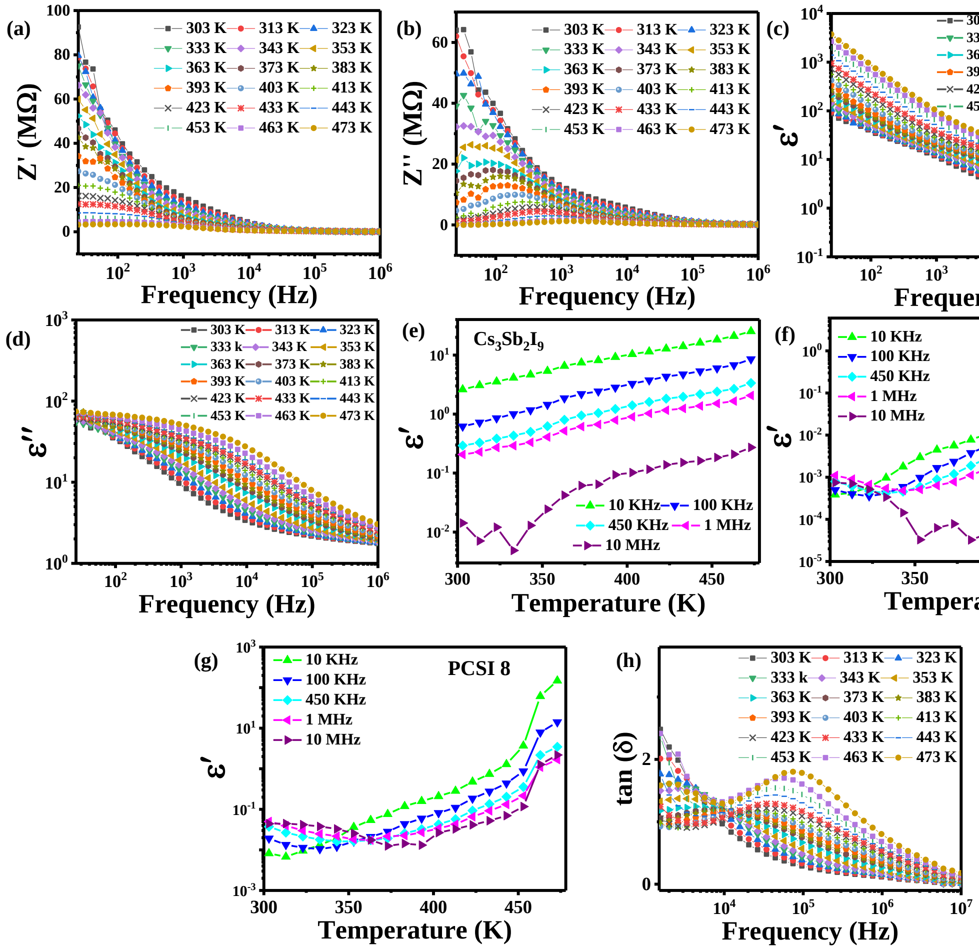

Figure S10: *Frequency-dependent (a) real part of impedance (Z′), (b) imaginary part of impedance (Z′′), (c) real part of dielectric constant (ϵ′), (d) dielectric loss (ϵ′′) at various temperatures of* $Cs_3Sb_2I_9$*, temperature-dependent real part of dielectric constant (ϵ′) of (e)* $Cs_3Sb_2I_9$*, (f) PVDF, (g) PCSI8, and (h) frequency-dependent loss tangent* $\tan(\delta)$ *at various temperatures.*

Fig. S10a illustrates how the real part of complex impedance, Z′(ω), varies with the frequency at different temperatures. In the low frequency region, Z′(ω) is high but it starts decreasing when the frequency increases for all temperatures. In high frequency region, Z′(ω) remains constant with the temperature, suggesting the release of space charges and a reduced role of grain boundaries in total impedance at high frequencies [1]. The reduction in Z′(ω) with increasing temperature might be due to the decreased trapped charge density and increased mobility of charge carriers. The imaginary part of complex impedance, Z′′(ω), is shown in Fig.

S10b. Z″(ω) vs ω is known as the loss spectrum which shows the distinct relaxation peaks at different temperatures. These peaks appear when the frequency of the external field matches with the localized hopping frequency of the electron. The shifting of the relaxation peak with increasing temperature suggests the presence of thermally activated charge carriers.

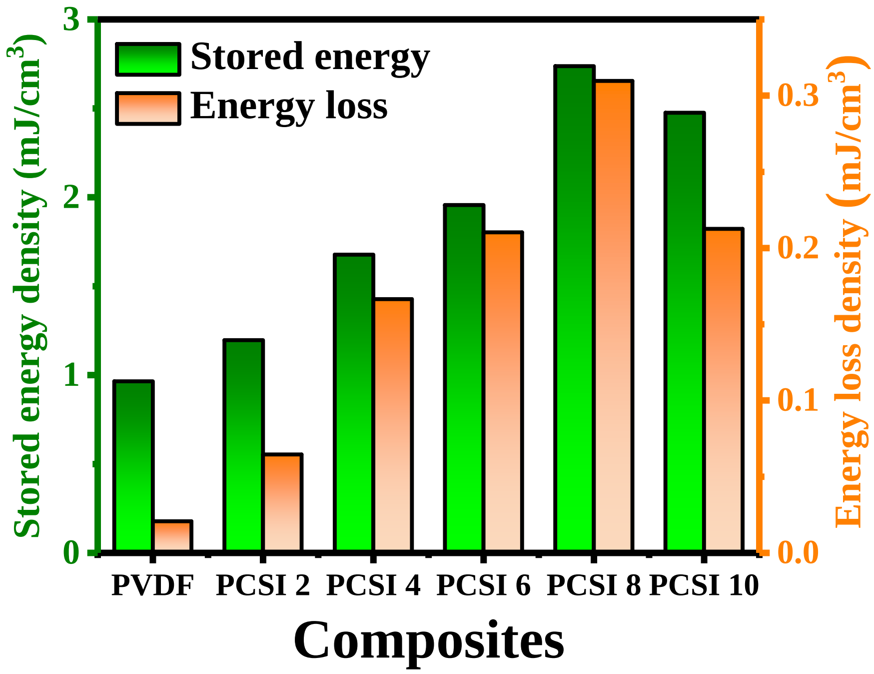

Figure S11: *The stored energy densities and energy loss densities of PVDF and all the PCSIs.*

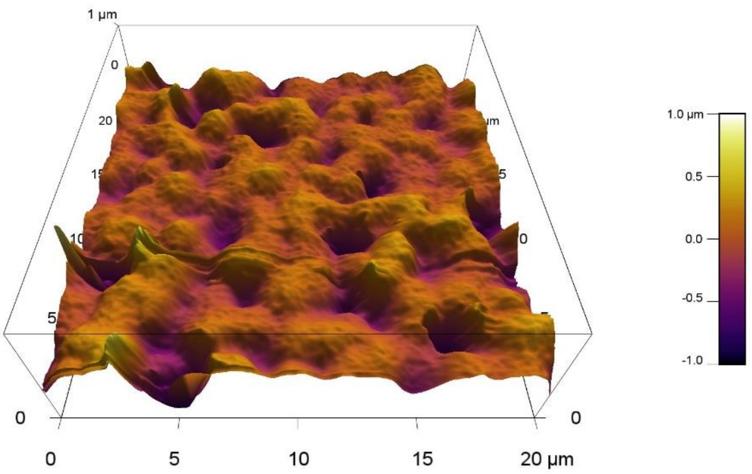

Figure S12: *The 3D AFM topographical image of PCSI8*

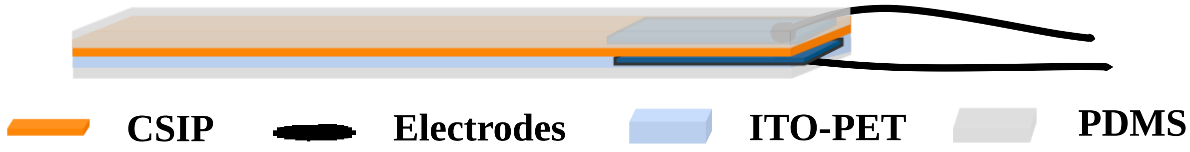

Figure S13: *Schematic of the piezoelectric nanogenerator device.*

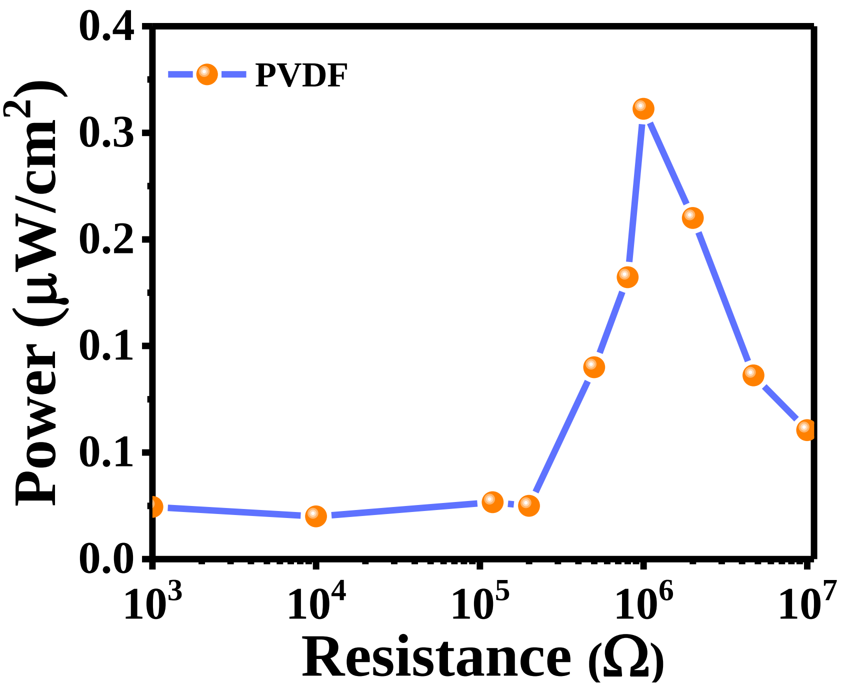

Figure S14: *Power density of PVDF*

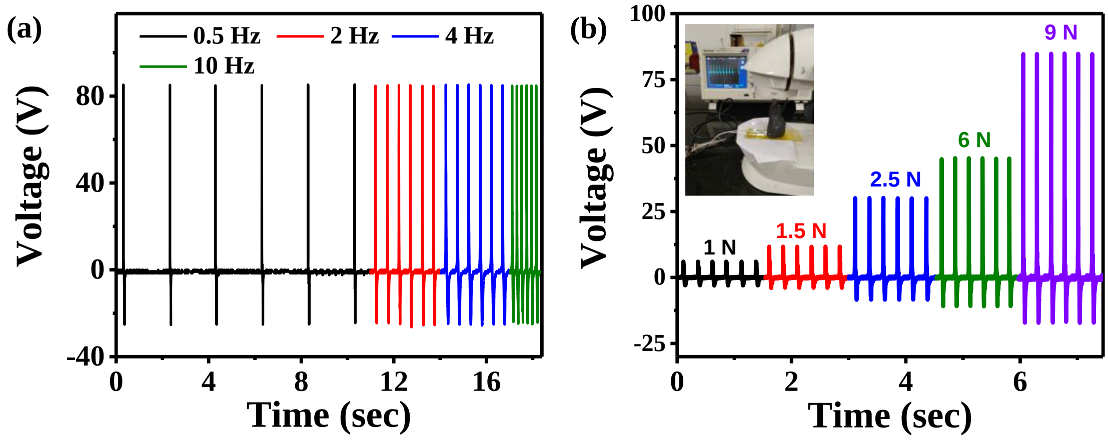

Figure S15: *Output voltage of PCSI 8 under (a) different frequencies and (b) different forces.*

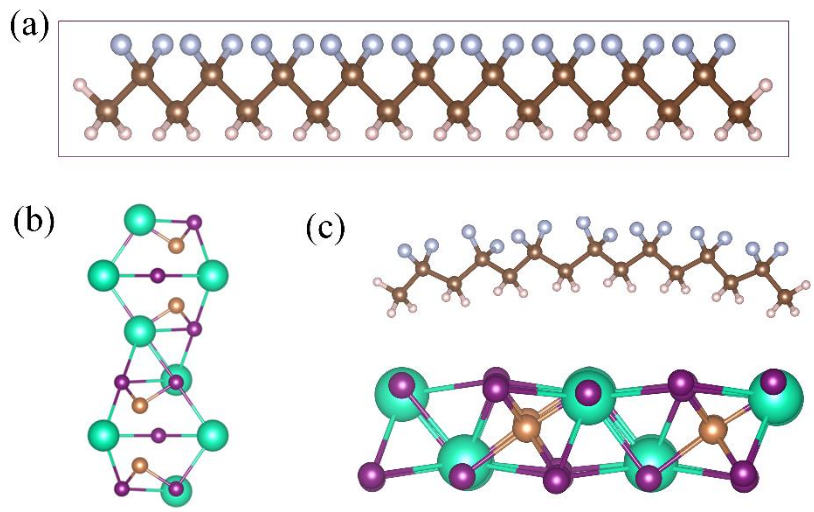

Figure S16: *Optimized structure of (a)* $Cs_3Sb_2I_9$*, (b) PVDF and (c)* $Cs_3Sb_2I_9$*-PVDF hetrostructure. Grey, white, silver, green, violet, brown sphere represent carbon, hydrogen, flourine, cesium, iodine and antimony respectively.*

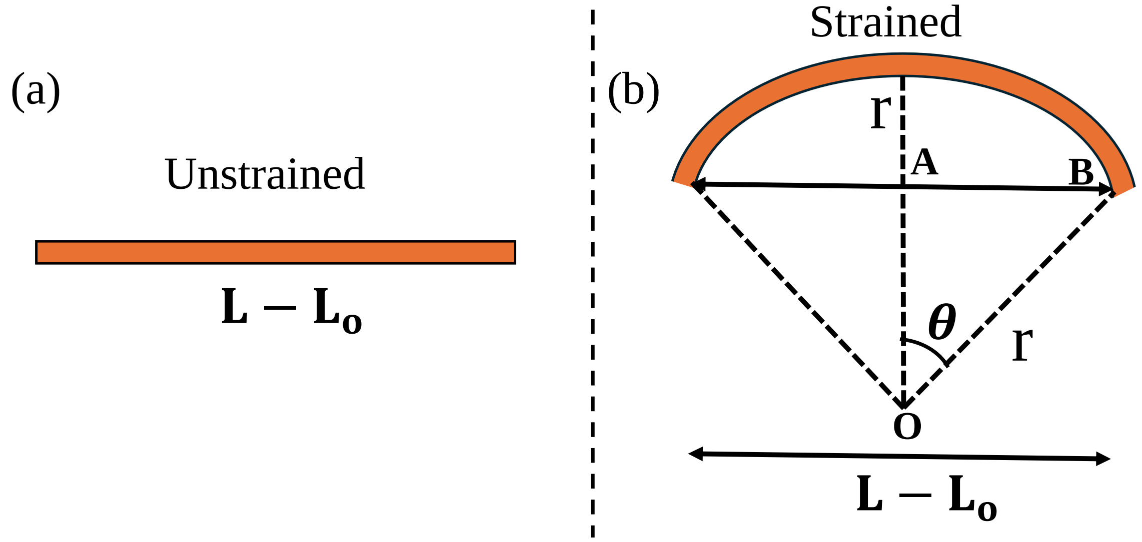

Figure S17: *The schematic representation of the film in (a) unstrained, and (b) strained conditions for the calculation of generated strain.*

From Fig. S17b, using the trigonometry relation in ΔOAB, the equation (4) in the main manuscript is derived as:

$$\sin\theta = \frac{(L - L_0)/2}{r}$$

$$L = r \cdot (2\theta)$$

$$sin\left(\frac{L}{2r}\right) = \frac{L - L_0}{2r}$$

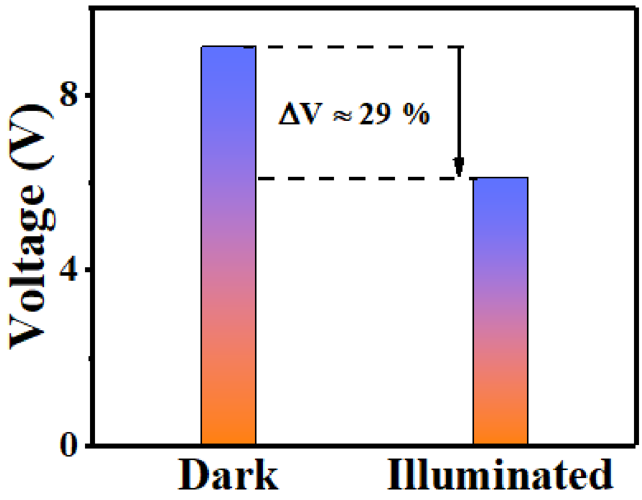

Figure S18: *Change in output voltage of the photodetector in dark and illuminated conditions.*

Table S1: Comparison of different nanogenerators

Polymer	Filler/Device Structure	Pressure/ Force	Output voltage	Current/ Current density	Applications	Stability/ Cycles	Reference
PVDF	$FAPbBr_3$	Finger imparting	26.2 V	2.1 µA	Calculator, LCD screen, speaker, and wristwatch	4 weeks	[2]
PVDF	$ErCl_3$. $6H_2O$ and $Fe(NO3)_3$, 9H2O	Finger imparting	115	32 µA	Glowing of LEDs	-	[3]
PVDF	$MAPbBr_3$	Finger touch	5 V	60 nA	Responses observed from NG as different letters	3600 cycles	[4]
PVDF	ZnO NRs	Bending	85 V	2.2 µA	Glowing of LEDs	-	[5]
PVDF	Graphene	2 Pa	11 V	6 nA/cm2	Velocity sensor	-	[6]
PDMS	ZnS/MWCNT	13.6 kPa	35 V	77.7 nA	Wrist watch, calculator, and LCD	-	[7]
PDMS	PZT	0.4 Mpa	22 V	-	Glowing of LEDs	3 days/6000 cycles	[8]
PVDF	Hexagonal boron nitride	Hard tapping	68 V	0.1 µA	-	1500 cycles	[9]
P(VDF – TrFE)	$CsPbBr_3$ QDs	0.6 Mpa	11.5 V	-	Powering LEDs	1200 cycles	[10]
PEDOT coated PVDF		8.3 kPa	48 V	6 µA	Weight measurement Mapping, Vibration Sensor, Fatigue Testing	21000 cycles	[11]
PVDF	**$Cs_3Sb_2I_9$**	**Hand hammering**	**85 V**	**2.6 µA**	**Capacitor charging, Glowing of LEDs**	**10000 cycles**	**This Work**

References:

[1] Pu Y, Dong Z, Zhang P, Wu Y, Zhao J, Luo Y. Dielectric, complex impedance and electrical conductivity studies of the multiferroic $Sr_2FeSi_2O_7$-crystallized glass-ceramics. Journal of Alloys and Compounds 2016;672:64–71. https://doi.org/10.1016/j.jallcom.2016.02.137.

[2] Si SK, Paria S, Karan SK, Ojha S, Das AK, Maitra A, et al. In situ-grown organo-lead bromide perovskite-induced electroactive γ-phase in aerogel PVDF films: an efficient photoactive material for piezoelectric energy harvesting and photodetector applications. Nanoscale 2020;12:7214–30. https://doi.org/10.1039/D0NR00090F.

[3] Hoque NA, Thakur P, Roy S, Kool A, Bagchi B, Biswas P, et al. Er^{3+}/Fe^{3+} Stimulated Electroactive, Visible Light Emitting, and High Dielectric Flexible PVDF Film Based Piezoelectric Nanogenerators: A Simple and Superior Self-Powered Energy Harvester with Remarkable Power Density. ACS Appl Mater Interfaces 2017;9:23048–59. https://doi.org/10.1021/acsami.7b08008.

[4] Sultana A, Alam MdM, Sadhukhan P, Ghorai UK, Das S, Middya TR, et al. Organo-lead halide perovskite regulated green light emitting poly(vinylidene fluoride) electrospun nanofiber mat and its potential utility for ambient mechanical energy harvesting application. Nano Energy 2018;49:380–92. https://doi.org/10.1016/j.nanoen.2018.04.057.

[5] Li J, Chen S, Liu W, Fu R, Tu S, Zhao Y, et al. High Performance Piezoelectric Nanogenerators Based on Electrospun ZnO Nanorods/Poly(vinylidene fluoride) Composite Membranes. J Phys Chem C 2019;123:11378–87. https://doi.org/10.1021/acs.jpcc.8b12410.

[6] Garain S, Jana S, Sinha TK, Mandal D. Design of In Situ Poled Ce3+-Doped Electrospun PVDF/Graphene Composite Nanofibers for Fabrication of Nanopressure Sensor

and Ultrasensitive Acoustic Nanogenerator. ACS Appl Mater Interfaces 2016;8:4532–40. https://doi.org/10.1021/acsami.5b11356.

[7] Sultana A, Alam MdM, Garain S, Sinha TK, Middya TR, Mandal D. An Effective Electrical Throughput from PANI Supplement ZnS Nanorods and PDMS-Based Flexible Piezoelectric Nanogenerator for Power up Portable Electronic Devices: An Alternative of MWCNT Filler. ACS Appl Mater Interfaces 2015;7:19091–7. https://doi.org/10.1021/acsami.5b04669.

[8] Park K-I, Jeong CK, Ryu J, Hwang G-T, Lee KJ. Flexible and Large-Area Nanocomposite Generators Based on Lead Zirconate Titanate Particles and Carbon Nanotubes. Advanced Energy Materials 2013;3:1539–44. https://doi.org/10.1002/aenm.201300458.

[9] Yadav P, Raju TD, Badhulika S. Self-Poled hBN-PVDF Nanofiber Mat-Based Low-Cost, Ultrahigh-Performance Piezoelectric Nanogenerator for Biomechanical Energy Harvesting. ACS Appl Electron Mater 2020;2:1970–80. https://doi.org/10.1021/acsaelm.0c00272.

[10] Nie J, Zhu L, Zhai W, Berbille A, Li L, Wang ZL. Flexible Piezoelectric Nanogenerators Based on P(VDF-TrFE)/$CsPbBr_3$ Quantum Dot Composite Films. ACS Appl Electron Mater 2021;3:2136–44. https://doi.org/10.1021/acsaelm.1c00137.

[11] Maity K, Mandal D. All-Organic High-Performance Piezoelectric Nanogenerator with Multilayer Assembled Electrospun Nanofiber Mats for Self-Powered Multifunctional Sensors. ACS Appl Mater Interfaces 2018;10:18257–69. https://doi.org/10.1021/acsami.8b01862.